ACS APPLIED MATERIALS & INTERFACES

Letter

www.acsami.org

Peptide Nucleic Acid (PNA)–DNA Duplexes: Comparison of Hybridization Affinity between Vertically and Horizontally Tethered PNA Probes

Arpita De,[†] Serhiy Souchelnytskyi,[‡] Albert van den Berg,[†] and Edwin T. Carlen*[,†]

[†]BIOS Lab on a Chip Group, MESA+ Institute for Nanotechnology, University of Twente, Enschede, The Netherlands

[‡]Department of Oncology and Pathology, Karolinska Institute, Stockholm, Sweden

Supporting Information

ABSTRACT: We compare the PNA–DNA duplex hybridization characteristics of vertically tethered and new horizontally tethered PNA probes on solid surfaces. The horizontal 15-mer PNA probe has been synthesized with linker molecules attached at three locations (γ-points) positioned along the PNA backbone that provides covalent attachment of the probe with the backbone aligned parallel to the surface, which is important for DNA hybridization assays that use electric field effect sensors for detection. A radioactive labeled assay and real-time surface plasmon resonance (SPR) biosensor are used to assess the probe surface density, nonspecific binding, and DNA hybridization affinity, respectively, of the new PNA probe configuration. The estimated equilibrium dissociation constants of the horizontally tethered duplex and the vertically tethered duplex are of the same order of magnitude ($K_D \approx 5$ nM), which indicates a sufficient hybridization affinity for many electronic biosensors that benefit from the horizontal alignment, which minimizes the effects of counterion screening.

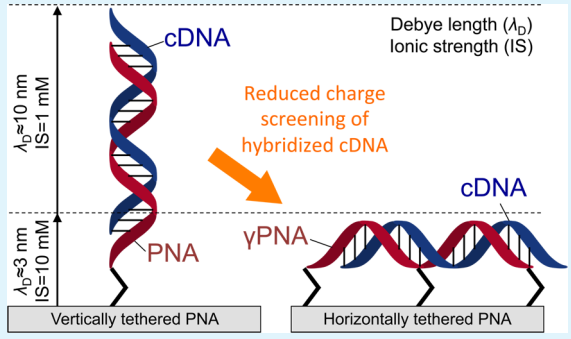

KEYWORDS: *PNA, γ-PNA, chiral backbone, counterion screening, surface hybridization*

Molecular assays based on the hybridization of target DNA to complementary DNA oligomer probes attached to a solid surface were first reported nearly four decades ago,[1] and have since been applied extensively to the measurement of gene expression using microarrays[2] and molecular diagnostics using biosensors.[3] Stable DNA duplexes are readily formed in high ionic strength buffers because of the relaxation of the electrostatic repulsion of the complementary strands, which promotes interstrand complementary base pairing.[4−6] Synthetic DNA-like molecules, peptide nucleic acid (PNA), locked nucleic acid (LNA), and phosphoramidate morpholino (MORF) oligomers have been reported over the last several years for improved DNA and RNA hybridization performance. LNAs include a modification to the ribose sugar unit of the nucleotide that retains the negative charge from the phosphate backbone and provides highly specific RNA sequence recognition and do not suffer from aggregation problems typically associated with PNA.[7,8] MORFs are uncharged probes for DNA hybridization, where six-membered morpholino rings replace the ribose sugar, and a nonionic phosphordiamidate linkage replaces the negatively charged phosphodiester backbone. The MORFs are reported to be better suited for gene expression applications because they can be synthesized with up to 70 nucleotides,[9] compared to LNA and PNA. In this article, we are interested in PNA probes because of their synthesis flexibility, and specifically the incorporation of chiral units along the carbon chains of the molecule backbone that provide unique molecular configurations for functional group attachment and conjugation to solid surfaces.[10−12] PNA probes, which form PNA–DNA complementary duplexes according to established Watson–Crick base pairing rules, have been reported to have higher affinity and sequence selectivity compared to conventional DNA–DNA duplex hybridization.[13] PNA is an uncharged DNA mimic where the negatively charged phosphodiester backbone of DNA (Figure 1a) is replaced with an achiral 2-amino-ethyl-glycine (AEG) backbone (Figure 1b).[14]

The improvement in thermodynamic stability of the PNA–DNA duplex has been attributed to the lack of electrostatic repulsion in the backbone[14] and another contribution may come from counterion release upon hybridization, as opposed to condensation taking place within DNA.[15] In addition, the AEG backbone is highly resistant to enzymatic degradation from nucleases and proteases that are widely used for regulating gene expression.[16] Other applications for PNA include the identification of single nucleotide polymorphism,[17] and isolation and purification of nucleic acids.[18]

Received: March 29, 2013
Accepted: May 13, 2013
Published: May 13, 2013

   dx.doi.org/10.1021/am4011429 | *ACS Appl. Mater. Interfaces* 2013, 5, 4607–4612

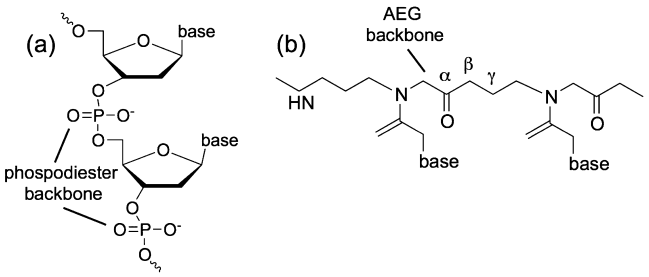

Figure 1. Backbone structures: (a) DNA, (b) PNA.

Surface-immobilized PNA probes are particularly important for biosensor applications because of the PNA–DNA duplex stability and their flexibility for synthesis into different configurations, especially for field-effect transistor (FET) sensors, such as silicon nanowire sensors,[19−21] which measure the intrinsic charge of hybridized complementary DNA to surface-immobilized PNA probes on the gate-oxide sensor surface in the form of an increase in surface charge density. Conventional DNA and PNA probes have been attached to the gate-oxide surface using various chemical cross-linking strategies, which result in DNA or PNA probes extended vertically away from the sensor surface. For electronic biosensors, such as FET sensors that measure the net intrinsic electronic charge of the hybridized duplex on the sensor surface, there is a fundamental problem due to counterion screening at the gate-oxide surface[22−24] and counterion condensation of the negatively charged DNA,[6] which can significantly reduce the net detectable surface charge. The length of the counterion screening layer, the Debye length λ_D, is dependent on the ionic strength of the hybridization buffer; a high ionic strength results in a small λ_D and charge screening beyond ∼1−2 nm above the gate-oxide surface,[22,23] which means that electronic charge extending beyond λ_D from the sensor surface will be effectively screened and will not be transduced into a measurable sensor signal.

Initial reports indicated that low ionic strength buffers, where λ_D is large enough to preclude counterion screening, did not negatively affect the PNA–DNA hybridization affinity;[19,20] however, it was later reported that PNA–DNA hybridization kinetics favor high to moderate ionic strength buffers.[25] Therefore, conventional vertically extended PNA–DNA duplex detection sensitivity is affected by counterion screening in a similar way as DNA–DNA hybridization.[23] It has also been reported that the hybridization of DNA to surface adsorbed DNA probes with the backbone aligned parallel, or horizontal, to the sensor surface is more effective for the electronic detection of DNA compared to vertically tethered complementary probes as the electronic charge of the duplex is minimally screened by counterions in the hybridization buffer at the gate-oxide surface.[26,27] However, previous reports used physically adsorbed DNA probes on the gate-oxide surface, whereas covalently attached probe molecules are better-suited for molecular assays. Our group has previously reported silicon nanowire chemical sensors,[28] and biosensors for the measurement of PNA–DNA hybridization detection, where the PNA probe was attached to the silicon nanowire surface using a conventional vertical orientation, in low ionic strength buffer.[21]

Previous research on PNA backbone modification at the α and γ positions (Figure 1b) has been reported to increase the selectivity of complementary DNA recognition due to the presence of chiral centers.[29] Furthermore, studies of γ-modified PNAs revealed that the introduction of a side chain in this position does not hinder formation of DNA and RNA duplexes; and the insertion of the modified PNA into a standard PNA oligomer induces structural organization and allows for an improvement in the binding affinity.[10,30] In fact, the modification to the PNA backbone at the chiral γ positions gives an inherent helicity to the PNA making it more rigid, thus easier to form a duplex with DNA.[10] The γ modifications to the backbone can also provide functional end groups for rotating the molecule such that the PNA probe can be covalently attached with horizontal alignment to the sensor surface using a conventional aldehyde amine reduction attachment scheme.[31] Figure 2 shows a comparison between a vertical PNA–DNA duplex with single end-point covalent PNA attachment (Figure 2a) and a horizontal PNA–DNA duplex with three covalent attachment points conjugated to the three γ points in the PNA backbone and their relation to the Debye length λ_D (Figure 2b). Therefore, hybridized PNA–DNA duplexes aligned parallel to the gate-oxide surface will also be minimally affected by counterions in moderately high ionic strength buffers, which is required for fast and selective hybridization kinetics. Furthermore, the horizontal probe alignment does not limit the probe length, as is the case with the conventional vertically tethered probe.

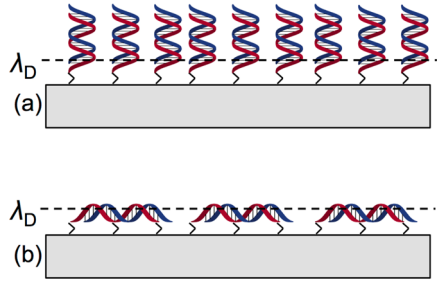

Figure 2. Qualitative PNA–DNA duplex hybridization formats and relation to the Debye length λ_D. (a) vertical PNA probes with single end-point attachment (b) horizontal PNA probes with three γ attachment points.

Two different 15-mer PNA probe molecules have been synthesized with three γ attachment points along the backbone of the PNA molecule, as shown in Figure 3. At each γ point, a 2-aminoethoxy-2-ethoxy acetic acid (AEEA) linker molecule, with length 1.3 nm, is terminated with an amine group (Figure 3a) that is used to conjugate the γ-PNA to a silicon dioxide (SiO_2) surface using the reduction of silane aldehyde surface groups with sodium-cyano-borohydride ($NaCNBH_3$) (see Scheme S2 in the Supporting Information). For attachment to Au surfaces, a hydrocarbon chain with thiol end group (C6-SH) linker, with length approximately 1.1 nm, is used to attach the γ-PNA probe (Figure 3b).

The attachment density and binding affinity of the horizontally tethered γ-PNA probes are estimated and compared to conventional vertically extended PNA probes tethered to the solid support surface with a single end attachment point. The attachment density is performed on cleaned SiO_2 pieces and the PNA and γ-PNA probes are covalently attached in 1 μM concentrations using a small volume reaction vessel that is clamped to the surface. The PNA and γ-PNA functionalized surfaces are exposed to complementary (M0) DNA, labeled with a P^{32} radioisotope for surface density estimation, in a phosphate buffer with varying ionic

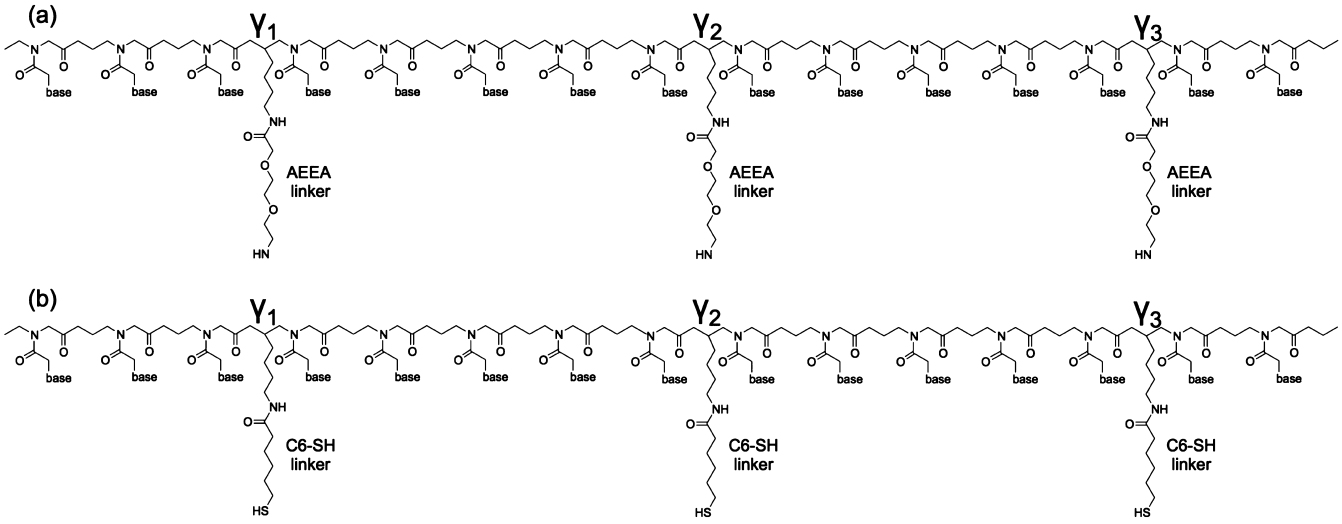

Figure 3. γ-PNA molecules with linker molecules attached at three γ-points (γ_1,γ_2, and γ_3) on the AEG-backbone: (a) 2-aminoethoxy-2-ethoxy acetic acid (AEEA) with amine end group for attachment to SiO_2 surfaces; (b) hydrocarbon chain linker with thiol end group (C6-SH) for attachment to Au surfaces.

strength (1, 23, and 137 mM) at pH 7.4 for 1 h without stirring (static hybridization) in a 50 μL volume reaction vessel. The posthybridization surfaces are washed with the same hybridization buffers and a final wash with high ionic strength buffer (1 M NaCl). For both cases, the posthybridization surface densities are $\sim 1 \times 10^{12}$ duplexes cm^{-2} without significant changes for all three ionic strength buffers. A point can be made that the γ-PNA presented here with three γ points spread across the 15-mer sequence in the backbone (Figure 3) are not clumped together as in a chiral box,[32,33] which although constrained, favor specific antiparallel duplex[30] with high ionic strength buffer.[25] The posthybridization surface densities are similar for the case of flowing the radiolabeled M0 DNA over the PNA functionalized surfaces for 10 min (see Figures S1 and S2 in the Supporting Information). Additionally, nonspecific binding to the PNA and γ-PNA functionalized surfaces is assessed using noncomplementary (NC) DNA-P[32] and is strongly dependent on the conformation of attachment end groups, which will be discussed later.

The hybridization kinetics of the PNA–DNA and γ-PNA–DNA duplex formation are assessed by estimating the equilibrium dissociation constant K_D from real-time hybridization measurements from a conventional imaging surface plasmon resonance (SPR) instrument. Since the SPR measurement surface is Au, the thiolated PNA and γ-PNA probes are used for attachment. The cysteine from the PNA probe provides the thiol group for attachment to the Au surface in an end-tethered vertical configuration. The γ-PNA, with C6-SH linkers attached to the three γ-points on the backbone (Figure 3b), is conjugated to the Au SPR sensors. The kinetics experiments are performed in a flow-cell with a flow velocity of $v \sim 0.5$ mm s^{-1}, thus in the reaction-limited regime,[34] and the measured data is fit to the Langmuir model in two steps to estimate the association rate constant k_a (M^{-1} s^{-1}), which represents the speed of the second-order probe-target interaction, and the dissociation rate k_d (s^{-1}), which represents the speed of the first-order breakdown of the probe-target complex. The equilibrium dissociation constant is defined as $K_D = k_d/k_a$ (M) and a small, typically less than about 10 nM, K_D value indicates a high affinity of the target for the probe molecule. The extracted dissociation constants are listed in Table 1 (see Figures S3 and S4, Supporting Information).

Table 1. Estimated PNA–DNA and γ-PNA–DNA Duplex Hybridization Dissociation Constant

duplex	k_a ($\times 10^5$ M^{-1} s^{-1})	k_d ($\times 10^{-4}$ s^{-1})	K_D (nM)
PNA–DNA (M0)	0.6	2	3
γPNA–DNA (M0)	0.9	4	5

The extracted dissociation constant for the PNA–DNA duplex is larger than the previously reported value of 1.2 nM for 15-mer PNA–DNA duplexes attached to the Au surface with two series-connected AEEA linker molecules.[35] Because the DNA sample concentrations are much larger than the K_D, the affinity measurements performed in this letter are used to compare the hybridization performance between the PNA–DNA and γ-PNA–DNA duplexes. The extracted K_D for the γ-PNA–DNA duplex is of the same order of magnitude as the conventional PNA–DNA, which is encouraging since the γ-PNA probe has restricted movement due to the three-point tethered surface attachment. It has been suggested that γ-PNA–DNA duplexes would be unstable in the case of surface hybridizations with chiral PNA probes;[36,37] however, in this case, the γ-PNA–DNA is slightly different from chiral PNA as it does not contain consecutive chiral points on the backbone, i.e., "chiral box". The measured $K_D \approx 5$ nM for γ-PNA–DNA in this case is in fact significantly smaller than the reported polylysine-DNA–DNA horizontal surface hybridization of $K_D \approx 200$ nM,[26] and therefore, our approach is applicable for the covalent attachment of horizontally aligned PNA probes for electronic biosensors. Also because of the restricted conformation of the surface attached γ-PNA, it discriminates noncomplementary DNA (NC DNA) from complementary DNA (M0) in all ionic strength situations (see Figure S1 in the Supporting Information).

Another important property of the PNA probe molecule is the surface attachment density and we evaluate two different schemes for the attachment of PNA and DNA probes on SiO_2 surfaces (see Figure S1, in the Supporting Information). Aminated DNA probes (Am-DNA P[32]) are attached to the

dx.doi.org/10.1021/am4011429 | ACS Appl. Mater. Interfaces 2013, 5, 4607–4612

SiO_2 surface via reduction of the silane aldehyde surface groups with $NaCNBH_3$[31] and thiolated DNA probes (Th-DNA-P^{32}) are attached to SiO_2 using maleimide activation on 3-amino-propyl-triethoxy-silane (APTES) covered SiO_2 surface. The Am-DNA-P^{32} attachment provides a probe surface density of $N_s \sim 10^{10}$ molecules cm^{-2} and the Th-DNA-P^{32} attachment provides a probe surface density $N_s \approx 5 \times 10^{12}$ molecules cm^{-2}, which is in agreement with reported values of surface probe density for the respective attachment schemes.[38,39] Although the Th-DNA attachment scheme requires a longer surface preparation time of 8−12 h[38] compared to the Am-DNA attachment scheme that requires 3−4 h,[31] the Th-DNA is the preferred attachment method for electronic biosensors as a larger N_s results in a larger transduced signal,[27] and a surface density of 5×10^{12} molecules cm^{-2} is reported to be well-suited for good hybridization efficiency.[40,41] The surface attachment density of PNA attachment to SiO_2 surfaces is evaluated using a Cy5 fluorescence label for both aminated attachment (Am-PNA-Cy5) and thiolated attachment (Th-PNA-Cy5). The surface density for Am-PNA-Cy5 is $N_s \approx 0.5 \times 10^{12}$ molecules cm^{-2} and for Th-PNA-Cy5 is $N_s \approx 1 \times 10^{12}$ molecules cm^{-2}. The Am-DNA-P^{32} and Am-PNA-Cy5 probe densities differ by an order of magnitude and the discrepancy is related to the nonspecific adsorption of Am-PNA to SiO_2 surfaces, which is a known characteristic of PNA due to the uncharged backbone,[35−37] and is critically important for surface hybridization assays.

To confirm the nonspecific adsorption of the different PNA attachment schemes to the SiO_2 surfaces, PNA was incubated on SiO_2 surfaces without a cross-linking/reducing agent and subsequently imaged using the radioactive and fluorescence labels previously described. The Am-PNA was incubated on SiO_2 surfaces functionalized with silane aldehyde without any $NaCNBH_3$ coupling buffer, and Th-PNA incubated on the SiO_2 surface treated with APTES without cross-linking. Both surfaces were sonicated in deionized water for 15 min and exposed to complementary DNA-P^{32} for hybridization. Each surface was subsequently washed with a 1 M NaCl posthybridization buffer and measured. The Am-PNA−DNA hybridization density is 0.4×10^{12} molecules cm^{-2}, which is the same order of magnitude as the previous surface density measurements of Am-PNA-Cy5 and clearly confirms the nonspecific adsorption of the Am-PNA to the SiO_2 surfaces.[37] The surface density of Th-PNA nonspecifically adsorbed to the APTES coated SiO_2 is an order of magnitude less than the covalently coupled Th-PNA probe and can be explained by the fact that an APTES coated SiO_2 surface is slightly positively charged due to the protonated amine groups at pH 7. It has been reported that polylysine and polyaspartate differentially attach electrostatically to hafnium oxide deposited on SiO_2 because of the same principle of amine protonation of amines in polylysine and deprotonation of aspartates at pH >7.[42] The nonspecific adsorption results are summarized in Table 2.

Table 2. Nonspecific Adsorption of Am-PNA and Th-PNA to SiO_2 Surfaces

complex	surface density ($\times 10^{12}$ molecules cm^{-2})
Am-PNA−DNA-P^{32}	0.38
Am-PNA-Cy5	0.41
Th-PNA-Cy5	0.02

On the basis of these observations, we evaluated other material surfaces commonly used for biosensor manufacturing, including silicon nitride (Si_3N_4), polyimide (PI) and poly dimethyl-siloxane (PDMS), by hybridizing DNA-P^{32} to surfaces that have been incubated with Am-PNA probe molecules. Following the hybridization step, the surfaces are washed with a high ionic strength wash buffer and sonicated for 15 min. The Am-PNA probes were directly incubated in deionized water on the respective surfaces without any treatment with silane aldehyde, APTES, or cross-linker. The surface density of DNA-P^{32} hybridized to PNA nonspecifically adsorbed to the Si_3N_4 surface is 0.4×10^{12} molecules cm^{-2}, to the PI surface is 0.2×10^{12} molecules cm^{-2}, and on the PDMS surface is 4×10^{12} molecules cm^{-2}, all of which are quite significant. The nonspecific adsorption of γ-PNA to the four surfaces was evaluated similarly by measuring the surface density of DNA-P^{32} hybridized to the nonspecifically adsorbed γ-PNA to SiO_2, Si_3N_4, polyimide, and PDMS, and the postsonicated surface densities are 0.7×10^{12}, 0.9×10^{12}, 1×10^{12}, and 0.6×10^{12} molecules cm^{-2}, respectively.

In summary, PNA−DNA hybridization on solid surfaces is promising for biosensor applications because of its stability and flexibility for synthesis into different configurations; however, careful consideration of the surface attachment scheme and surfaces is required for their use in practical applications. We present a new γ-PNA surface probe for electronic biosensors with the backbone aligned parallel to the sensor surface, thus minimizing the counterion screening effect when high ionic strength hybridization buffers are used for optimal hybridization kinetics. The γ-PNA−DNA binding affinity is of the same order of magnitude as the conventional PNA−DNA hybridization binding affinity performed using the same experimental conditions, however, is sufficient for practical applications. Furthermore, we have evaluated two commonly reported attachment schemes and report that a thiolated attachment scheme is preferred as it provides significantly larger probe surface density and negligible nonspecific adsorption of PNA to most materials.

EXPERIMENTAL SECTION

Chemicals. All reagents and solvents used were of analytical grade and used without further purification. 3-amino-propyl-triethoxy-silane (APTES), tris-ethanolamine (TEA) hydrochloride, and sodium cyanoborohydride (NaCNBH3) were purchased from Sigma Aldrich. Trimethoxysilane aldehyde was purchased from United Chemical Technologies. Sulfo-succinimidyl 4-(N-maleimidomethyl)cyclohexane-1-carboxylate (sulfo-SMCC) was purchased from Pierce. The polydimethyl-siloxane (PDMS) prepolymer (Sylgard, Dow Corning). Purified peptide nucleic acids (PNA) were purchased from Panagene, Korea, and the DNA oligomers were purchased from Eurogentec.

Radiolabeling of Oligonucleotides. The DNA was radiolabeled with (γ-^{32}P)-ATP at the 5′ end using a T4 polynucleotide kinase (T4 PNK) using a protocol from New England Biolabs.[25] The T4 polynucleotide kinase was purchased from Sigma (10 units μL^{-1}, 500 UN), (γ-^{32})-ATP (BLU002250UC, 10 Ci $mmol^{-1}$, 2 mCi mL^{-1}, 250 μCi). The 1 × T4 PNK buffer consists of 70 mM Tris-HCl, 10 mM $MgCl_2$, and 5 mM DTT at pH 7.6. Briefly, the labeling process consisted of a 50 pmol DNA sample in a 50 μL reaction volume that was reacted with 20 enzyme units in the 1 × T4 PNK buffer for 1 h at 37 °C, and followed by direct ethanol

Table 3. Sequences of PNA and DNA Used for Experiments

molecule/complex	sequence
PNA	Cys-TGT-ACA-TCA-CAA-CTA-NH_2
Am-γ-PNA	Ac-TGT*(AEEA)-ACA-TC*(AEEA)A-CAA-C*(AEEA)TA
Th-γ-PNA	Ac-TGT*(C6-SH)-ACA-TC*(C6-SH)A-CAA-C*(C6-SH)TA-3′
complementary (M0) DNA	5′-TAG-TTG-TGA-TGT-ACA-3′
Am-DNA	5′-TAG-TTG-TGA-TGT-ACA-3′-NH_2
Th-DNA	5′-TAG-TTG-TGA-TGT-ACA-3′-SH
noncomplementary (NC) DNA	5′-ATC-AAC-ACT-ACA-TGT-3′

precipitation of the radiolabeled DNA. All radiolabeling experiments were done under adequate radiation protection in a radioactive material handling certified laboratory (BL4 laboratory). Precipitated radiolabeled oligomers were washed with 70% three times until the Geiger counter measuring the signal was constant. Constant signal indicated that nonreacted isotope was washed away and only labeled probe was collected.

PNA Probe Surface Attachment. SiO_2 samples with 1 cm^2 surface area were used for the surface probe density studies with fluorescently labeled PNA (PNA-Cy5) and radiolabeled DNA oligomers. The probes were covalently attached to the SiO_2 surface in a 5 mm diameter reaction vessel formed from a 4 mm thick PDMS layer to avoid droplet evaporation effects during immobilization. PDMS well chips were cut out with a knife and punched (5 mm, Harris-Unicore) from a PDMS (10:1 PDMS to curing agent ratio) slab cured on a blank silicon wafer. The PDMS wells were cleaned by sonicating in ethanol. A 50 μL probe solution was incubated in the PDMS-SiO_2 well chip in a humidity chamber. Subsequent reaction and washing steps were done inside the reaction vessel. Two types of attachment chemistry were followed, using two different silanes and end groups on SiO_2 that bind aminated and thiolated probes. Thiolated probes were coupled to APTES treated SiO_2 surfaces. Briefly piranha cleaned SiO_2 surfaces were treated with 2% APTES in 95% ethanol for 1 h, washed in ethanol and heated to 120 °C for 15 min. APTES-coated SiO_2 is activated with 5 mM heterobifunctional cross-linker sulfo-SMCC in 10 mM TEA buffer pH 7.2 for 1 h yielding a maleimide terminated surface to couple 1 μM thiolated probes in TEA buffer pH 7.2 for 12 h in a humidity chamber. Aminated probes were functionalized to silane aldehyde treated SiO_2 surfaces. Briefly, piranha cleaned SiO_2 surfaces were treated with 2% silane aldehyde in 95% ethanol for 1 h., washed in ethanol, and heated to 120 °C for 15 min. Silane aldehyde conjugated to SiO_2 surfaces was reacted with 1 μM aminated probe with the 4 mM $NaCNBH_3$ reducing agent in 10 mM phosphate buffer pH 8.4 for 2 h. The silane aldehyde on SiO_2 surfaces is reduced to reductive alkylation to form a secondary amine with the aminated probe. A Phosphorus imager (Storm 860, Molecular Dynamics) was used for radioisotope detection from radiolabeled and sonicated surfaces. Because PNA cannot be radiolabeled, the probe surface attachment density of the aminated and thiolated probes has been estimated using radiolabeled oligomers, as well as fluorescence (aminated, Am-PNA-Cy5; and thiolated, Th-PNA-Cy5). Fluorescent measurements were performed using the Bio-Rad Molecular FX scanner. In addition to the SiO_2 surfaces, other surfaces including silicon nitride (Si_3N_4), polyimide (PI), and PDMS have also been tested for nonspecific binding of probes after washing and sonication.

Two kinds of PNA probes have been used for surface functionalization. Conventional vertically tethered PNA with achiral polyamide backbone made up of repeating N-(2-amnioethyl) glycine units, whereas the horizontally tethered PNA probes (γ-PNA) use a substituent, usually corresponding to the side chain of a natural amino acid, inserted into the γ position of the PNA backbone (Figure 3). The γ-PNA probe (designed and synthesized by Panagene) consisted of the same sequence as the conventional PNA and was designed with respect to favorable position of the γ-substituents in the backbone of the PNA. In our experiments, the PNA and γ-PNA have the same sequences and differ with three γ-substituted lysine residues in the backbone of the PNA. The PNA molecule has a single amine group available for end functionalization to surfaces in a vertical orientation. An ethylene glycol linker (AEEA) is added together with the γ-lysine residues in the PNA backbone to enhance solubility of the molecule.

Hybridization Density Measurements. SiO_2 surfaces were functionalized with one of the two schemes using thiolated and aminated PNA probes and hybridized to radiolabeled complementary M0 and noncomplementary NC DNA in 1 mM phosphate buffer with varying NaCl concentrations (1, 23, and 137 mM). DNA was allowed to hybridize to the surface functionalized PNA probes for 1 h in static condition and in separate experiments for 10 min in a PDMS microchannel with a flow rate of 7 μL min^{-1}. For static hybridization (PDMS well based method) 10:1 PDMS was cured on a flat silicon wafer, then small area (1 cm^2) PDMS squares were cut out and punched with a punching tool (5 mm diameter, Harris Uni-Core). The square PDMS pieces with the hole were cleaned by sonication in ethanol, followed by assembly on SiO_2 pieces as hybridization vessel. For hybridization in flow, a PDMS microfluidic chip with microchannel (1 cm in length and 360 μm diameter) was clamped onto the probe functionalized SiO_2 surface. Radiolabeled DNA was transported though the microchannel using a 250 μL syringe (Hamilton Gastight) with a syringe pump (Standard PHD Ultra, Harvard Apparatus). The inlet and outlet holes were punched into the PDMS chip with punch tool (0.5 mm, Harris-Uni-Core) and a 1 cm long stainless steel tubing with 700 μm OD could easily make a tight fit as inlet and outlet tubing. These 700 μm diameter tubing were further connected via 500 μm ID Tygon tubing and connected to the syringe using 150 μm ID PEEK tubing with appropriate fittings (Upchurch Scientific).

Surface Plasmon Resonance Measurements. The real-time PNA–DNA and γ-PNA–DNA hybridization measurements were done using a commercially available imaging surface plasmon resonance (SPR) instrument (SPRImageII, GWC Instruments). The SPR measurements were performed using SPR imaging substrates (SPRchip GWC). The PNA and γ-PNA were functionalized on the Au surface prior to conducting the experiments. Briefly, the SPR imaging substrates were first cleaned with a fresh piranha solution and subsequently rinsed with deionized water. The cleaned sensor substrates were then incubated with PNA for 12 h in PDMS well of 50 μL volume in a humidity chamber. The cysteine on the N-end of the PNA provides the thiol group for Au attachment, and for the C6-SH linker from the γ-PNA provided attachment to the Au surface. Probe functionalized SPR chips were mounted on the base of a prism with index matching oil

(n = 1.72, Cargille Laboratories), with the gold side facing the flow cell. Binding was monitored with the SPR imaging instrument. All PNA−DNA hybridization was monitored in 1 × PBS buffer with pH 7.4. The measured real-time SPR data is used to fit to the Langmuir kinetic model for affinity parameter extraction for the PNA−DNA binding. The measured SPR data was modeled with commercial software (Scrubber, BioLogic Software).

■ ASSOCIATED CONTENT

Supporting Information

Results for radioactive surface density measurements and equilibrium dissociation constant measurements and data extraction. This material is available free of charge via the Internet at http://pubs.acs.org/.

■ AUTHOR INFORMATION

Corresponding Author

*E-mail: e.t.carlen@utwente.nl.

Notes

The authors declare no competing financial interest.

■ ACKNOWLEDGMENTS

The authors thank Dr. Bob Pinedo for guidance and assistance. Thanks also to Johan Bomer, Jan van Nieuwkasteele, and Hans de Boer for technical assistance with silicon nanowire fabrication and the design and implementation of the measurement setup. This work was supported by the Nanopill project that was funded by a private cancer foundation in The Netherlands, and the Spinoza Prize from the Nederlandse Organisatie voor Wetenschappelijk Onderzoek (NWO). The radiolabeling work was performed in the Souchelnytskyi Group at the Karolinska Institute and was supported by EurocanPlatform, the Swedish Cancer Research Foundation, the Swedish Research Council, and the Radiumhemmet Research Foundation.

■ REFERENCES

(1) Southern, E. M. *J. Mol. Biol.* **1975**, *98*, 503−517.
(2) Kohane, I. S.; Kho, A.; Butte, A. J. *Microarrays for an Integrative Genomics*; MIT Press: Cambridge, MA, 2003.
(3) Piscevic, D.; Knoll, W.; Tarlov, M. J. *Supramol. Sci.* **1995**, *2*, 99−106.
(4) Casey, J.; Davidson, N. *Nucleic Acids Res.* **1977**, *4*, 1539−1552.
(5) Kaiser, W.; Rant, U. *J. Am. Chem. Soc.* **2010**, *132*, 7935−7945.
(6) Manning, G. S. *Q. Rev. Biophys.* **1978**, *11*, 179−246.
(7) Petersen, M.; Wengel, J. *Trends Biotechnol.* **2003**, *21*, 74−81.
(8) Demidov, V. V. *Trends Biotechnol.* **2003**, *21*, 4−7.
(9) Tercero, N.; Wang, K.; Gong, P.; Levicky, R. *J. Am. Chem. Soc.* **2009**, *131*, 4953−4961.
(10) Dragulescu-Andrasi, A.; Rapireddy, S.; Frezza, B. M.; Gayathri, C.; Gil, R. R.; Ly, D. H. *J. Am. Chem. Soc.* **2006**, *128*, 10258−10267.
(11) Rapireddy, S.; He, G.; Roy, S.; Armitage, B. A.; Ly, D. H. *J. Am. Chem. Soc.* **2007**, *129*, 15596−15600.
(12) Rapireddy, S.; Bahal, R.; Ly, D. H. *Biochemistry* **2011**, *50*, 3913−3918.
(13) Egholm, M.; Buchardt, O.; Christensen, L.; Behrens, C.; Freier, S. M.; Driver, D. A.; Berg, R. H.; Kim, S. K.; Norden, B.; Nielsen, P. E. *Nature* **1993**, *365*, 566−568.
(14) Nielsen, P. E.; Egholm, M.; Berg, R. H.; Buchardt, O. *Science* **1991**, *254*, 1497−1500.
(15) Tomac, S.; Sarkar, M.; Ratilainen, T.; Wittung, P.; Nielsen, P. E.; Norden, B.; Graslund, A. *J. Am. Chem. Soc.* **1996**, *118*, 5544−5552.
(16) Hanvey, J. C.; Peffer, N. J.; Bisi, J. E.; Thomson, S. A.; Cadilla, R.; Josey, J. A.; Ricca, D. J.; Hassman, C. F.; Bonham, M. A.; Au, K. G.; Carter, S. G.; Bruckenstein, D. A.; Boyd, A. L.; Noble, S. A.; Babiss, L. E. *Science* **1992**, *258*, 1481−1485.
(17) Lundin, K. E.; Good, L.; Strömberg, R.; Gräslund, A.; Smith, C. I. E. *Adv. Genet.* **2006**, *56*, 1−51.
(18) Gaylord, B. S.; Massie, M. R.; Feinstein, S. C.; Bazan, G. C. *Proc. Natl. Acad. Sci. U.S.A.* **2005**, *102*, 34−39.
(19) Hahm, J. I.; Lieber, C. M. *Nano Lett.* **2004**, *4*, 51−54.
(20) Zhang, G. J.; Zhang, G.; Chua, J. H.; Chee, R. E.; Wong, E. H.; Agarwal, A.; Buddharaju, K. D.; Singh, N.; Gao, Z.; Balasubramanian, N. *Nano Lett.* **2008**, *8*, 1066−1070.
(21) De, A.; van Nieuwkasteele, J.; Carlen, E.; van den Berg, A. *Analyst* **2013**, *138*, 3221−3229.
(22) Sørensen, M. H.; Mortensen, N. A.; Brandbyge, M. *Appl. Phys. Lett.* **2007**, *91*, 102105−102108.
(23) Stern, E.; Wagner, R.; Sigworth, F. J.; Breaker, R.; Fahmy, T. M.; Reed, M. A. *Nano Lett.* **2007**, *7*, 3405−3409.
(24) Elnathan, R.; Kwiat, M.; Pevzner, A.; Engel, Y.; Burstein, L.; Khatchtourints, A.; Lichtenstein, A.; Kantaev, R.; Patolsky, F. *Nano Lett.* **2012**, *12*, 5245−5254.
(25) Park, H.; Germini, A.; Sforza, S.; Corradini, R.; Marchelli, R.; Knoll, W. *Biointerphases* **2007**, *2*, 80−88.
(26) Bunimovich, Y. L.; Shin, Y. S.; Yeo, W. S.; Amori, M.; Kwong, G.; Heath, J. R. *J. Am. Chem. Soc.* **2006**, *128*, 16323−16331.
(27) Fritz, J.; Cooper, E. B.; Gaudet, S.; Sorger, P. K.; Manalis, S. R. *Proc. Natl. Acad. Sci. U.S.A.* **2002**, *99*, 14142−14146.
(28) Chen, S.; Bomer, J. G.; Carlen, E. T.; van den Berg, A. *Nano Lett.* **2011**, *11*, 2334−2341.
(29) Pensato, S.; Saviano, M.; Romanelli, A. *Expert Opin. Biol. Ther.* **2007**, *7*, 1219−1232.
(30) Dragulescu-Andrasi, A.; Zhou, P.; He, G.; Ly, D. H. *Chem. Commun.* **2005**, 244−246.
(31) Patolsky, F.; Zheng, G.; Lieber, C. M. *Nat. Protoc.* **2006**, *1*, 1711−1724.
(32) Corradini, R.; Feriotto, G.; Sforza, S.; Marchelli, R.; Gambari, R. *J. Mol. Recognit.* **2004**, *17*, 76−84.
(33) Manicardi, A.; Calabretta, A.; Bencivenni, M.; Tedeschi, T.; Sforza, S.; Corradini, R.; Marchelli, R. *Chirality* **2010**, *22*, E161−E172.
(34) Zimmermann, M.; Delamarche, E.; Wolf, M.; Hunziker, P. *Biomed. Microdevices* **2005**, *7*, 99−110.
(35) Cattani-Scholz, A.; Pedone, D.; Blobner, F.; Abstreiter, G.; Schwartz, J.; Tornow, M.; Andruzzi, L. *Biomacromolecules* **2009**, *10*, 489−496.
(36) Masuko, M. *Nucleic Acids Res. Suppl.* **2003**, *3*, 145−146.
(37) Weiler, J.; Gausepohl, H.; Hauser, N.; Jensen, O. N.; Hoheisel, J. D. *Nucleic Acids Res.* **1997**, *25*, 2792−2799.
(38) Chrisey, L. A.; Lee, G. U.; O'Ferrall, C. E. *Nucleic Acids Res.* **1996**, *24*, 3031−3039.
(39) Zammatteo, N.; Jeanmart, L.; Hamels, S.; Courtois, S.; Louette, P.; Hevesi, L.; Remacle, J. *Anal. Biochem.* **2000**, *280*, 143−150.
(40) Peterson, A. W.; Heaton, R. J.; Georgiadis, R. M. *Nucleic Acids Res.* **2001**, *29*, 5163−5168.
(41) Herne, T. M.; Tarlov, M. J. *J. Am. Chem. Soc.* **1997**, *119*, 8916−8920.
(42) Fahrenkopf, N. M.; Rice, P. Z.; Bergkvist, M.; Deskins, N. A.; Cady, N. C. *ACS Appl. Mater. Interfaces* **2012**, *4*, 5360−5368.